THRUST FAULTING IN THE THAUMASIA REGION AND IMPLICATIONS FOR THE STRUCTURE OF THE EARLY MARTIAN LITHOSPHERE. M. Grott, E. Hauber, *Institute of Planetary Research, German Aerospace Center (DLR), Berlin, Germany (matthias.grott@dlr.de, ernst.hauber@dlr.de)*, S.C. Werner, *Institute of Geoscience, Free University Berlin, Berlin, Germany*, P. Kronberg, *Institute of Geology, Technical University of Clausthal, Clausthal-Zellerfeld, Germany*.

Introduction: In the absence of in situ measurements the mechanical response of the lithosphere to stress is one of the few clues we have to the (paleo) surface heat flow of a planet, enabling us to reconstruct its thermal history. Here we will investigate lobate scarps in the Thaumasia region to gain insight into the thermal state of the early Martian lithosphere. The surface deformations associated with thrust faulting are largely controlled by the faulting geometry, i.e. by faulting angle and depth of faulting [1,2], and since the latter may be identified with an isotherm this allows us to constrain the thermal state of the seismic lithosphere at the time the scarps formed.

Observations: We consider two lobate scarps in the southern Thaumasia region on Mars, which is located at the southern rim of the Tharsis rise (Fig.1). The scarps are characterized by a steeply rising scarp face and a gently declining back scarp followed by a trailing syncline. We have taken two series of topographic profiles along the lines indicated in Fig.1, the results for the western scarp being displayed in Fig.2, where subsequent profiles have been offset by 500 m for better readability. The scarp face and back scarps have slopes of $\sim 10^\circ$ and $\sim 1^\circ$, respectively, and the trailing depression is located 60 km behind the surface break. Note that there is also a regional slope of $\sim 0.25^\circ$, which will be removed in the modeling process.

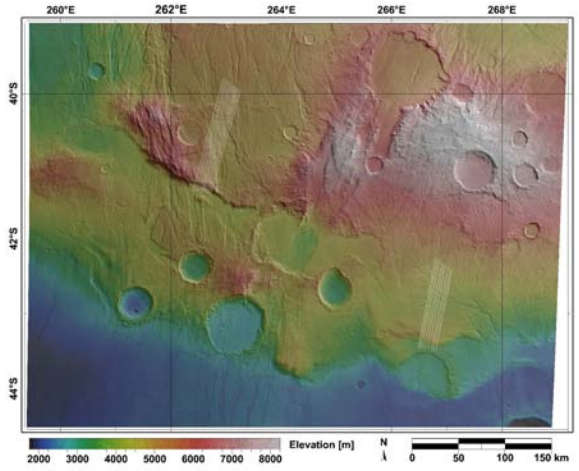

Figure 1: Topographic image map of the southern Thaumasia Region.

Methods: We use forward mechanical modeling to determine the surface displacement associated with the faulting. The approach is similar to the dislocation method [3], which has been applied to a wide range of tectonic problems including the simulation of thrust faults on Mercury and Mars [1,2].

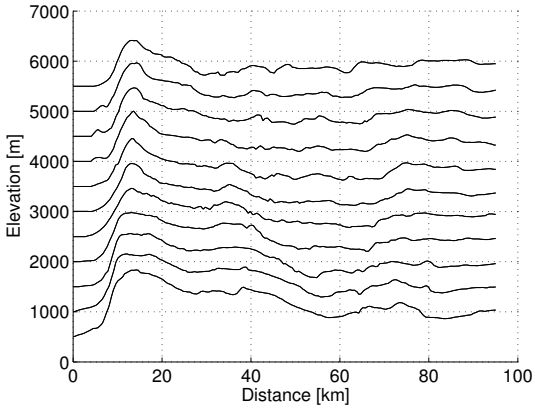

Figure 2: MOLA topographic profiles of the western lobate scarp taken along the lines indicated in Fig.1. For better readability subsequent profiles have been offset by 500 m.

We use the plane strain application mode of the commercial finite element package *FEMLAB* (http://www.femlab.com) to solve for the displacements resulting from slip on the fault. The model setup is given by an elastic half-space transected by a model fault which is specified by the angle θ and depth of faulting D as shown in Fig.3. The finite element mesh consists of approximately 18000 elements, which are refined at the surface and the fault plane, the maximum element size being 1 km and 500m, respectively. The fault is implemented as a gap whose boundaries are restricted to move in the tangential direction.

After specifying the fault geometry the distribution of slip on the fault surface is prescribed and the total amount of slip is increased until the total modeled relief matches the observed topographic offset. The displacements in the elastic half-space are calculated assuming values for Young's modulus and Poisson ratio of 100 GPa and 0.33, respectively. The simulations are carried out for $D = 20 - 40$ km and $\theta = 20 - 40^\circ$, the step sizes being 1 km and 2°, respectively. This allows for a systematic study of the trade off effects between θ and D and is achieved by use of the *MATLAB* (http://www.mathworks.com) interface to *FEMLAB*, which allows for a complete automatisation of the calculations once the initial model has been set up.

The surface topography is very sensitive to the specified slip distribution on the fault and tapered slip distributions having minimum slip at the fault tips are usually prescribed. Here we use a triangular taper with maximum slip near the surface break, as other choices fail to reproduce the steeply rising scarp face. The simulated surface deformation is then compared to

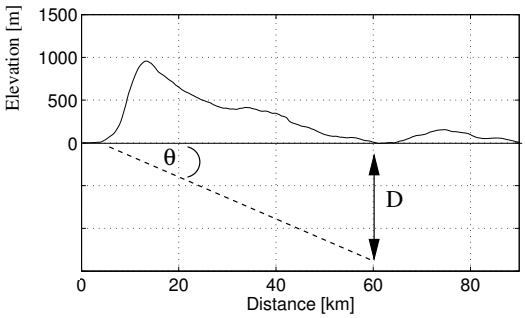

Figure 3: A sketch of the model geometry indicating the fault plane by a broken line. The depth D and angle of faulting θ are indicated.

the measured MOLA topography by aligning the positions of the corresponding trailing synclines. This approach is more robust than calculating for example the l^2-norm of the difference between the two profiles as it is less sensitive to the detrending carried out during data processing.

The method has been verified by reexamining the Amenthes Rupes thrust fault, which has been studied previously [1]. Using the presented approach the angle and depth of faulting are constrained to 25°-35° and 32-40 km, respectively. [1] report best fitting parameters of 30°-35° and 35-40 km, values withing the error margins determined here.

On Earths continents the maximum depth of intra-plate earthquakes is constrained by the transition from the frictionally unstable to the conditionally stable regime, a transition which coincides with the onset of plasticity of the corresponding rock [4]. This transition occurs when the stresses necessary to initiate sliding along preexisting cracks (seismic slip) become larger than those needed for ductile deformation (aseismic slip). Given the rheology of the rocks and the depth of the transition, the isotherm corresponding to this depth may be calculated by

$$T_{BDT} = \frac{Q}{nR}\left[\ln\left(\frac{fg\rho DA^{\frac{1}{n}}}{\dot{\varepsilon}^{\frac{1}{n}}}\right)\right]^{-1} \quad (1)$$

where n , Q, A are rheological parameters, R is the gas constant, g is surface gravity, f the frictional coefficient, D depth of the brittle ductile transition and $\dot{\varepsilon}$ strain rate. Given surface Temperature T_s and thermal conductivity k, the crustal heat flow at the time of scarp emplacement may then be calculated using Fourier's Law.

Results and Conclusions: Fig.4 shows the mean topographic profile (broken line) and best fit synthetic profile (solid line) obtained for a faulting angel of 30° and a depth of faulting 32 km for the western scarp. The spread of the measured profiles is indicated by the dotted lines. The method produces good fits to the observed surface deformation including the steeply sloping scarp face, gently dropping back scarp and position of the trailing syncline. The height of the base of the syncline with respect to the reference level also depends on the faulting angle, where low angles give smaller offsets. However, since the level of offset is a strong function of the background topographic gradient, this misfit cannot serve as a further constraint on the faulting geometry.

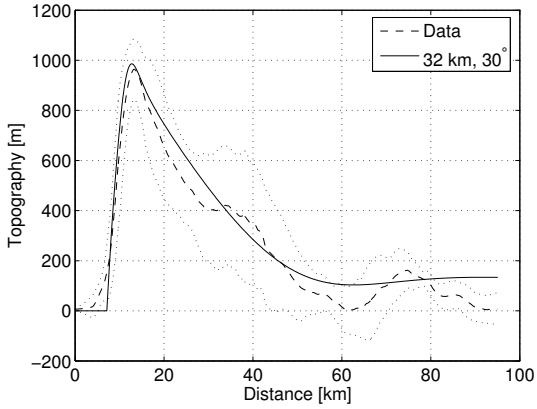

Figure 4: The mean topographic profile (broken line) and best fit synthetic profile obtained for a faulting angel of 30° and depth of faulting of 32 km for the western scarp. The mean spread of the measured profiles is indicated by the dotted lines.

The range of seismic layer thicknesses thus determined for the two scarps are 27-35 km (western) and 21-28 km (eastern scarp), allowing for a misfit of the position of the trailing syncline of 2 km. Assuming a diabase composition of the crust, a thermal conductivity of 2 W m^{-1} K^{-1} and a surface temperature of 220 K, the thermal gradients at the time of scarp formation were 12-18 K km^{-1} and 15-23 K km^{-1}, corresponding to heat flows of 24-36 and 30-46 mW m^{-2}, respectively.

These values fall within the range of Noachian heat fluxes that have been previously determined (14-20 K km^{-1} [1], >20 K km^{-1} [5], 27-33 K km^{-1} [6]). However, to serve as useful constraints on thermal evolution models, the times of scarp emplacement need to be determined more accurately. This will be done using crater statistics and is work in progress.

References: [1] Schultz R.A. and Watters T.R. (2001), *Geophys. Res. Lett.*, [2] Watters T.R. et al. (2002), *Geophys. Res. Lett.*, 29, 37-1. 28, 4659-4662. [3] Cohen S.C. (1999), *Adv. Geophys.*, 41, 133-231. [4] Scholz, C.H. (1998), *Nature*, 391, 37-42. [5] McGovern P.J. et al (2004), *J. Geophys. Res.*, 109, E07007. [6] Grott M. et al. (2005), *Geophys. Res. Lett.*, 32, L21201, doi:10.1029/2005GL023894.